Biosensors and Bioelectronics: X 26 (2025) 100663

Contents lists available at ScienceDirect

Biosensors and Bioelectronics: X

journal homepage: www.journals.elsevier.com/biosensors-and-bioelectronics-x

Optimization of a portable ligand-free optical spectroscopy method for SARS-CoV-2 protein detection

Fatin Hamimi Mustafa [a,*], Nik Yusnoraini Yusof [b], Mawaddah Mohd Azlan [b], Fariza Hanim Suhailin [c,h], Chan Yean Yean [d], Nik Mohd Noor Nik Zuraina [d], Mohd Zulkifli Salleh [d], Hironaga Uchida [e], Irneza Ismail [f], Rosline Hassan [g], Raja Kamarulzaman Raja Ibrahim [c,h], Mohd Adzir Mahdi [i]

[a] Department of Electronic & Computer Engineering, Faculty of Electrical Engineering, Universiti Teknologi Malaysia, 81310, Johor Bahru, Johor, Malaysia
[b] Institute for Research in Molecular Medicine (INFORMM), Universiti Sains Malaysia Health Campus, Kubang Kerian, 16150, Kelantan, Malaysia
[c] Department of Physics, Faculty of Science, Universiti Teknologi Malaysia, 81310 Skudai, Johor, Malaysia
[d] Department of Medical Microbiology and Parasitology, School of Medical Sciences, Universiti Sains Malaysia, 16150, Kubang Kerian, Kelantan, Malaysia
[e] Department of Electrical and Electronic Information Engineering, Faculty of Engineering, Toyohashi University of Technology, Japan
[f] Department Electrical & Electronic Engineering, Faculty of Engineering and Built Environment, Universiti Sains Islam Malaysia, Bandar Baru Nilai, 71800, Negeri Sembilan, Malaysia
[g] Department of Hematology, School of Medical Sciences, Universiti Sains Malaysia, 16150, Kubang Kerian, Kelantan, Malaysia
[h] Laser Center, Ibnu Sina Institute for Scientific and Industrial Research (ISI-SIR), Universiti Teknologi Malaysia, 81310 Skudai, Johor Bahru, Malaysia
[i] Wireless and Photonic Networks Research Centre, Faculty of Engineering, Universiti Putra Malaysia (UPM), Serdang 43400, Selangor, Malaysia

ARTICLE INFO

Keywords:
COVID-19
SARS-CoV-2 protein
Ligand-free
Optical spectroscopy
Optical system optimization
COVID-19 clinical measurements

ABSTRACT

The rapid spread of COVID-19 has underscored the need for fast, portable, and reliable diagnostic tools. Conventional techniques such as polymerase chain reaction and emerging biosensors like surface plasmon resonance require complex procedures for ligand development and immobilization, which often involve probes, antibodies, or aptamers. This study proposes a ligand-free detection strategy based on optical spectroscopy for the rapid identification of the SARS-CoV-2 protein. The detection workflow includes two key phases: optimization and clinical validation. In the optimization phase, transmittance spectral measurements were conducted on SARS-CoV-2 protein to determine the optimal wavelength within the ultraviolet–visible–near infrared range (200–1100 nm). The most effective fiber configuration was also evaluated using three combinations of transmitter–receiver fiber diameters: 600–400 μm, 600–100 μm, and 200–400 μm. The optimal detection parameters were identified as 275 nm for wavelength and 600–400 μm for fiber configuration. Specificity testing confirmed complete discrimination between SARS-CoV-2 protein and other proteins, including SARS-CoV and rBmSXP, with 100 % specificity. Subsequently, clinical validation was conducted on 21 patients using the optimized parameters. Optical spectroscopy measurements were compared with real-time quantitative reverse transcription polymerase chain reaction (RT-qPCR), yielding a correlation coefficient of 0.6038 with statistical significance ($p < 0.01$). These findings demonstrate the potential of portable, ligand-free optical spectroscopy for rapid SARS-CoV-2 detection at the point of care.

1. Introduction

The World Health Organization (WHO) declared Coronavirus Disease 2019 (COVID-19) a global pandemic on March 11, 2020, following a rapid escalation of confirmed cases exceeding 200,000 and over 800 deaths across more than 130 countries (Cucinotta and Vanelli, 2020; Spinelli and Pellino, 2020). The initial outbreak was reported in Wuhan, China, in December 2019 (Khan et al., 2020), and within just three months, the virus had rapidly spread across most countries worldwide (Gössling et al., 2020). As of 2025, new COVID-19 cases continue to be reported daily in many regions, with a global death toll approaching six million (Sapuan et al., 2025). During the pandemic, many countries

This article is part of a special issue entitled: Point-of-Care Technologies and Biosensing published in Biosensors and Bioelectronics: X.

* Corresponding author.
E-mail address: fatinhamimi@utm.my (F.H. Mustafa).

https://doi.org/10.1016/j.biosx.2025.100663
Received 7 April 2025; Received in revised form 17 July 2025; Accepted 24 July 2025
Available online 28 July 2025

enforced curfews or lockdowns, severely restricting daily activities to curb the transmission of the virus. These public health interventions caused substantial disruptions to both economic activities and social engagement. COVID-19 is primarily transmitted through respiratory droplets and aerosols that are released by infected individuals during coughing, breathing, sneezing, or speaking. Infected individuals may present a wide spectrum of symptoms, ranging from asymptomatic to mild flu-like illness (e.g., fever), and in severe cases, respiratory distress (Yesudhas et al., 2021). Importantly, even asymptomatic individuals can also transmit the virus to vulnerable populations with weaker immune systems. Due to the highly contagious nature of SARS-CoV-2, effective disease control strategies require diagnostic tools that are not only rapid and accurate, but also portable.

COVID-19 is caused by a novel coronavirus known as severe acute respiratory syndrome coronavirus 2 (SARS-CoV-2). SARS-CoV-2 contains ribonucleic acid (RNA) at its core, which is bound to nucleocapsid proteins (N-proteins). This core is encapsulated by an outer lipid layer that is composed of membrane proteins. The membrane protein works as chemical transmitters and to maintain the structural integrity of the virus. Embedded alternately within the membrane are spike glycoproteins (S-proteins) and envelope proteins, with S-proteins being relatively larger in size (Hardenbrook and Zhang, 2022). In terms of detection, RNA serves as the unique molecular fingerprint of a virus, which encodes its specific genomic information (e.g., for SARS-CoV-2). Therefore, detection of viral RNA in clinical samples is a direct indication of viral presence in the host. One of the most widely used RNA-based diagnostic techniques is polymerase chain reaction (PCR), along with its advanced version, real-time quantitative reverse transcription PCR (RT-qPCR). PCR quantifies the presence of SARS-CoV-2 RNA by measuring the cycle quantification (*Cq*) value, following RNA extraction from patient swab samples (Liu et al., 2020). The PCR amplifies viral RNA through repeated cycles of denaturation, annealing, and synthesis—typically exceeding 40 cycles. A lower number of cycles (i.e., lower *Cq* value) or rapid RNA replication reflects a higher RNA concentration in the sample (Mustafa et al., 2023). Although PCR is regarded as the gold standard for COVID-19 detection, it is a laboratory-based technique that requires skilled personnel and is time-consuming (Lino et al., 2022).

During infection, human immune system produces antibodies that primarily target the viral S-proteins (Zhao et al., 2021). Additionally, antibodies can also be produced against N-protein. Individuals with weakened immune responses or reduced antibody production often experience more severe symptoms. In protein-based sensing, this principle of antibody–antigen interaction is replicated on sensor surfaces, as seen in lateral flow assays (LFA) and enzyme-linked immunosorbent assays (ELISA). These techniques (e.g., LFA and ELISA) detect binding between an immobilized ligand such as antibody or aptamer and the target SARS-CoV-2 protein (e.g., S-protein, N-protein) on the diagnostic surface (Di Domenico et al., 2021; Mahmoudinobar et al., 2021). Additionally, a secondary tag such as a fluorescent dye or horseradish peroxidase (HRP) enzyme is also attached to the protein to enable quantification of the binding event. However, a major drawback of protein-based detection is the requirement for external reading instruments, which limits its portability and usability in resource-limited settings.

The emergence of biosensing technologies, such as electrochemical sensors and surface-enhanced Raman spectroscopy (SERS), has garnered increasing attention due to their ability to perform direct measurements without the need for secondary labelling tags (Lee et al., 2023). Additional advantages of biosensors include ease of use, cost efficiency, portability, and seamless integration with computing platforms for Internet of Things (IoT) applications. Most biosensors share a common design principle involving functionalization and immobilization strategies. A functionalized sensing surface which is typically composed of substrates such as silica or electrodes are modified with nanomaterials, including gold nanoparticles (AuNPs) or doped graphene (Yano et al., 2022). These nanostructured platforms are subsequently immobilized with selective ligands (e.g., antibodies, probes, aptamers) to enable specific binding with target analytes or antigens (e.g., proteins, DNAs). The key distinction among biosensor types lies in their signal transduction mechanisms. For example, SERS relies on the enhancement of optical signals via localized surface plasmon resonance (Shim et al., 2022), whereas electrochemical sensors detect changes in electrical or electrochemical signals induced by biomolecular interactions at the sensor interface (Mojsoska et al., 2021). Recent advancements in functionalization techniques and ligand development have enhanced reproducibility and cost-effectiveness. For instance, a study by Wu et al. introduced butanol-assisted uniform self-assembly of AuNP–cDNA probes for SARS-CoV-2 detection using a SERS platform (note: RNA is converted into cDNA via reverse transcription to enable detection and improve molecular stability) (Wu et al., 2023). In another study that employs a similar SERS strategy, functionalized gold nanoneedles with antibodies were used to physically trap the SARS-CoV-2 S-protein (Yang et al., 2021). Separately, a low-cost aptamer-based electrochemical sensor for detecting the N-protein demonstrated successful measurements within 5 min of measurement times (Siu et al., 2024). Although these recent technologies have shown significant progress, their development procedures remain time-consuming and resource-intensive. Therefore, this study proposes an optical spectroscopy approach that offers a simplified workflow and eliminates the need for surface functionalization, ligand development, and immobilization steps.

Optical spectroscopy method utilizes light within the ultraviolet–visible–near infrared (UV–VIS–NIR) wavelength range of 200–2500 nm to directly interact with target samples (e.g., SARS-CoV-2 S-protein). The transmitted spectrum is then analyzed to determine the sample's molecular absorption characteristics (Tkachenko, 2006). The absorption of optical radiation by a specific target is highly dependent on its molecular composition, particularly the presence of functional groups such as O–H, C–H, and C=O bonds. At certain wavelengths, these molecular bonds undergo vibrational excitation as they absorb energy from the incident light. Optical spectroscopy has been explored in various viral detection studies and has demonstrated promising outcomes. For instance, a study on Zika viruses employing optical spectroscopy combined with an artificial neural network (ANN) achieved 97 % accuracy in distinguishing between uninfected and Zika-infected samples (Garcia et al., 2022). Another positive result was reported in influenza detection, where optical spectroscopy paired with soft independent modeling of class analogy (SIMCA) successfully identified influenza infection in all 33 patients (100 % accuracy) (Sakudo et al., 2012). In a separate study on human immunodeficiency virus (HIV), a strong correlation ($R > 0.8$) was observed between optical spectroscopy measurements and ELISA results across 12 subjects (Sakudo et al., 2005). Collectively, these findings highlight the significant potential of optical spectroscopy as a reliable tool for viral detection.

In this study, optical spectroscopy is employed to measure extracted SARS-CoV-2 S-proteins and clinical SARS-CoV-2 virus samples. First, the optimal detection wavelength for the SARS-CoV-2 S-protein is determined based on normalized transmittance (*%T*) spectra, corresponding to a prominent absorption peak. The influence of various system parameters is also assessed by altering the fiber diameters on both the transmission and reception sides. Subsequently, the specificity of the SARS-CoV-2 protein is evaluated using a principal component analysis (PCA) model by comparing it with proteins from other diseases that share similar clinical symptoms, such as fever, cough, and fatigue. These comparator proteins include the SARS-CoV protein and the rBmSXP protein, which are associated with respiratory infections from the coronavirus family and Brugia malayi, respectively (Zhou et al., 2021). Finally, a clinical study is conducted to determine the correlation between the transmittance (*%T*) measured by optical spectroscopy and the quantification cycle (*Cq*) values obtained from RT-qPCR. This study differs from the previous works on COVID-19 detection using optical spectroscopy, as those studies did not optimize the system to determine the most effective optical parameters. Most previous approaches directly

employed optical spectroscopy for clinical measurements without prior system refinement (Rumaling et al., 2023). In contrast, the present study optimizes both the detection wavelength and the fiber diameter configurations. Another key distinction lies in the choice of target analyte: this study focuses on the SARS-CoV-2 S-protein, whereas past studies targeted viral RNA (Kitane et al., 2021; Minamikawa et al., 2021) or N-protein (Coelho et al., 2024). Some studies even analyzed the whole virus directly without selecting a specific molecular target. In another study, optical spectroscopy was combined with electrostatic potential sensing, using immobilized antibodies bound to the N-protein onto aluminum electrodes that were attached to a cuvette (Al Ahmad et al., 2021). Although this opto-electrochemical assay demonstrated a promising figure of merit (FOM <1), it still required complex procedures involving ligand development and immobilization. In this study, targeting the S-protein using the optimized wavelength yields a relatively stronger optical response, as the large S-protein is located on the outermost surface of the SARS-CoV-2 virion. Furthermore, unlike earlier works that only distinguished between COVID-19-positive and negative samples, this study also considers other infectious diseases with overlapping clinical symptoms.

2. Experimental section

2.1. Preparation of SARS-CoV-2 protein and clinical SARS-CoV-2 samples

Samples of human coronavirus SARS-CoV-2 spike protein RBD (1 mg/mL, 50 μg; ab273065, Batch No.: GR3338712-8) and SARS-CoV envelope protein (1 mg/mL, 100 μg; ab270833, Batch No.: GR3424498-1) were purchased from Abcam. The recombinant BmSXP protein sample was obtained from the INFORMM biobank. All protein samples were stored at −80 °C prior to dilution and measurement. The spike protein, in particular, was chosen as it plays a critical role in host cell recognition and entry, making it a suitable biomarker for detection strategies. The rBmSXP protein, although parasitic in origin, shares overlapping symptoms such as fever and malaise with viral infections, which justifies its inclusion as a negative control.

Nasopharyngeal swab samples from COVID-19 patients were collected and immersed in viral transport media (VTM), then stored at −80 °C at the Department of Medical Microbiology and Parasitology, School of Medical Sciences, Universiti Sains Malaysia. The collection was carried out between 2021 and 2022. Total nucleic acids were extracted using the Genolution Nextractor® NX-48N automated DNA/RNA isolation system (Genolution Inc., Seoul, Korea), following the manufacturer's protocol. Approximately 60 μL of eluted nucleic acid was obtained from each sample and stored in 1.5 mL microcentrifuge tubes at −80 °C for subsequent amplification via RT-qPCR. The clinical sample collection and related research procedures were approved by the Human Research Ethics Committee (JEPeM), Hospital Universiti Sains Malaysia (Protocol No.: USM/JEPeM/COVID19-44).

2.2. Measurement of SARS-CoV-2 protein

SARS-CoV-2 spike protein was initially used as the target analyte to evaluate its optical characteristics in the absence of other viral components (e.g., RNA, membrane proteins) and to facilitate system optimization. Prior to measurement, SARS-CoV-2 protein, SARS-CoV protein, and rBmSXP protein were diluted in phosphate-buffered saline (PBS, pH 7.4) in the concentration ranging from 0 to 100 ng/μL in 20 ng/μL increments. A deuterium–halogen light source (AvaLight-DH-S, Avantes; 200–2500 nm) and a spectrometer (AvaSpec-ULS2048CL-EVO-RS-UA, Avantes; 200–1100 nm) were allowed to stabilize for 30 min. Reference and dark spectra were recorded using an empty quartz micro cuvette (two-window, 1 × 2 mm window size, 8.5 mm optical path height, 100 μL volume). Protein samples were introduced into the cuvette using a micropipette in ascending concentration order.

Optical radiation from the light source was transmitted through the sample via a sub-miniature assembly (SMA) optical fiber (Ocean Optics). Transmitted light was collected by a second SMA fiber and captured by the spectrometer. Spectral data were acquired using AvaSoft 8 software, with 16 measurements recorded for each sample. To optimize the fiber configuration, three combinations of *Tx–Rx* fiber core sizes were evaluated: 600–400 μm, 600–100 μm, and 200–400 μm. The purpose of testing on SMA fiber combinations is to systematically investigate light coupling efficiency and scattering losses impact on the transmittance spectra across a range of analyte concentrations. All measurements were performed in triplicate on separate days for each concentration, and data were recorded independently. The cuvette was thoroughly rinsed with ultrapure water between sample runs. The same procedure was repeated using SARS-CoV and rBmSXP proteins to assess specificity and comparative optical signatures.

2.3. Measurement of clinical SARS-CoV-2 samples

Reverse transcription quantitative polymerase chain reaction (RT-qPCR) was conducted to analyze clinical SARS-CoV-2 samples, and quantification cycle (*Cq*) values were obtained using the LyteStar™ 2019-nCoV RT-PCR kit (ADT Biotech, Selangor, Malaysia). Each 25 μL PCR reaction mixture contained 13.5 μL of Master Mix A, 6.5 μL of Master Mix B, 0.5 μL of internal control, and 5 μL of eluted nucleic acid extracted from viral transport media (VTM). The RT-qPCR cycling protocol was as follows: reverse transcription at 50 °C for 30 min, initial denaturation at 95 °C for 15 min, followed by 45 amplification cycles consisting of 95 °C for 15 s and 58 °C for 45 s. The same clinical samples were subsequently measured using the optical spectroscopy setup as described in Section 2.2, employing the optimized transmitter–receiver (*Tx–Rx*) fiber combination that has been identified in Section 2.2. The clinical SARS-CoV-2 samples were directly introduced into the cuvette for optical measurements without any prior preprocessing steps such as centrifugation, dilution, or filtration. This approach was intended to preserve the clinically relevant condition of the samples and to assess the practical applicability of the assay for potential point-of-care use. The micro cuvette was thoroughly cleaned and rinsed with ultrapure water prior to each sample measurement. All procedures involving clinical samples were conducted under biosafety conditions, adhering to institutional guidelines. Negative and positive controls were included during RT-qPCR amplification to ensure assay validity and to detect potential contamination or inhibition.

2.4. Data analysis

The optimal wavelength for SARS-CoV-2 protein detection was determined using a multivariate statistical method, which was Principal Component Analysis (PCA). The PCA was conducted using Unscrambler X software (v10.3, CAMO, Oslo, Norway). All protein samples across concentrations were visualized in a two-dimensional (2D) PCA score plot based on the first two principal components (PC1 and PC2), which capture the highest spectral variance. PCA was selected due to its capacity to reduce high-dimensional spectral data into principal axes, allowing visual clustering and discrimination among closely related protein signatures.

The optimal *Tx–Rx* fiber configuration was determined by calculating the change in %*T* per concentration unit (i.e., %/ng/μL) for three *Tx–Rx* combinations: 600–400 μm, 600–100 μm, and 200–400 μm. The %*T* versus concentration graphs were plotted using linear regression in MATLAB (R2023b; MathWorks, Natick, MA), with error bars representing standard deviations.

To assess clinical relevance, the correlation between %*T* values from optical spectroscopy and *Cq* values obtained from RT-qPCR was calculated in MATLAB. Statistical performance was evaluated based on the correlation coefficient (R) derived from an ordinary linear regression model, with %*T* treated as the dependent variable and *Cq* value as the

reference. All regression analyses were performed with 95 % confidence intervals, and p-values <0.05 were considered statistically significant.

3. Results and discussion

3.1. Optimization of optical spectroscopy system

The optimization focuses on three key attributes: wavelength, optical fiber core diameter, and specificity. The first optimization that involves wavelength, is illustrated by the normalized transmittance (*%T*) spectra of SARS-CoV-2 protein across the 200–1100 nm range, as shown in Fig. 1. Two distinct minima are observed in the spectra, indicating significant absorption features at approximately 275 nm and 970 nm. These correspond to the primary constituents of the SARS-CoV-2 protein and water (PBS), respectively (Antosiewicz and Shugar, 2016; Jacques, 2013). A clear inverse relationship between protein concentration and transmittance at 275 nm is evident, where higher protein concentrations result in greater light absorption, and consequently, lower *%T* values. Notably, the 0 ng/μL sample exhibits no pronounced absorption features at 275 nm, confirming the absence of the target analyte (S-protein) in the solution. The identification of 275 nm as the optimal detection wavelength suggests a dominant contribution from protein-specific chromophores to the observed signal. Furthermore, across the full spectrum, the curves exhibit minimal baseline fluctuation, reflecting the stability and reproducibility of the optical system. The secondary spectral minimum at approximately 970 nm, attributed to water absorption in the PBS buffer, may serve as an internal reference for background correction or signal normalization.

In practical applications, the absorbance ratio at 260 nm and 280 nm (A260/A280) is a standard metric used in molecular biology to assess the purity and concentration of nucleic acids and proteins (Desjardins and Conklin, 2010). Nucleic acids such as DNA and RNA typically exhibit strong absorption at 260 nm, whereas proteins absorb around 280 nm due to the presence of aromatic amino acids such as tryptophan, tyrosine, and phenylalanine. These amino acids, particularly phenylalanine and tyrosine have been identified as potential biomarkers for distinguishing COVID-19 cases ranging from mild to severe (Edelhoch, 1967). The slight shift in protein absorbance observed in this study (275 nm instead of 280 nm) may be attributed to variations in the relative composition of these aromatic residues in the SARS-CoV-2 protein. Specifically, phenylalanine is the most abundant (6.5 %), followed by tyrosine (5.5 %) and tryptophan (2.9 %) (Luporini et al., 2021). This contrasts in SARS-CoV, where Howard et al., found that, six out of fourteen amino acid residues were tryptophan and tyrosine, with tryptophan being more abundant than tyrosine, and phenylalanine being the least (Howard et al., 2008). The absorbance ratio at 260 nm and 280 nm in SARS-CoV-2 positive samples is further supported by the finding from Rumaling et al., where distinct absorbance peaks were observed at both wavelengths (Rumaling et al., 2023). However, their negative samples also exhibited similar peaks, most likely due to the used of specific type of sample buffer. In contrast, other studies have reported various absorbance peaks at 450 nm, 850 nm, 1100 nm, and 1350 nm (Coelho et al., 2024), as those measurements were conducted on whole SARS-CoV-2 virus samples without targeting any specific analyte.

Fig. 2 shows the normalized transmittance, *(%T)*, plotted against concentration of SARS-CoV-2 protein for three combinations of *Tx-Rx* optical fibers; 600–100 μm, 200–400 μm, and 600–400 μm. Among these, the 600–400 μm configuration exhibits the highest sensitivity, with a slope of 0.5336 % *T* reduction per 1 ng/μL, indicating superior responsiveness to the changes in analyte concentration. In comparison, the 600–100 μm and 200–400 μm combinations yield sensitivity values of 0.2406 %/(ng/μL) and 0.2046 %/(ng/μL), respectively. Although the 600-400 μm setup showed a relatively higher coefficient of variation (CV) of 8.89 % compared to the 600–100 μm (3.79 %) and 200–400 μm (6.31 %) configurations, all values remained within the acceptable threshold for analytical applications (CV < 10 %) (Selinger et al., 2014). Additionally, the smaller error bars associated with the 600–400 μm setup further support its stability and reproducibility across repeated measurements. Considering both sensitivity and consistency, the 600–400 μm configuration was selected as the optimal fiber setup for subsequent experiments.

Although several previous studies on COVID-19 detection have reported sensitivity enhancement using optical fibers with smaller core diameters, such improvements are typically linked to specialized fiber

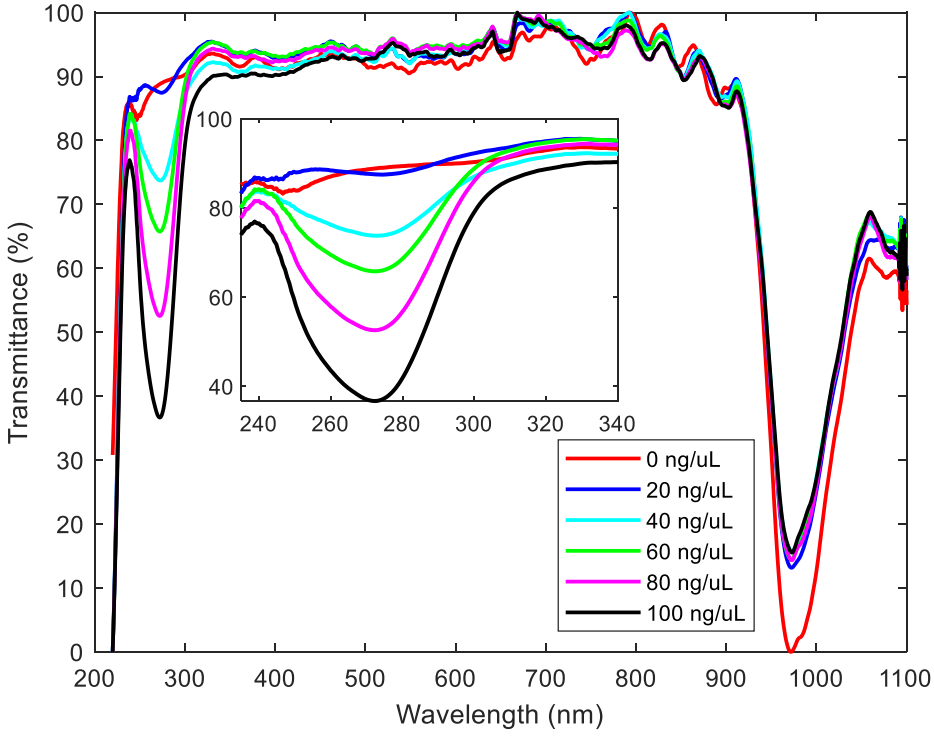

Fig. 1. Normalized transmittance (*%T*) spectra of the SARS-CoV-2 protein in different concentration from 0 ng/μL to 100 ng/μL in 20 ng/μL intervals.

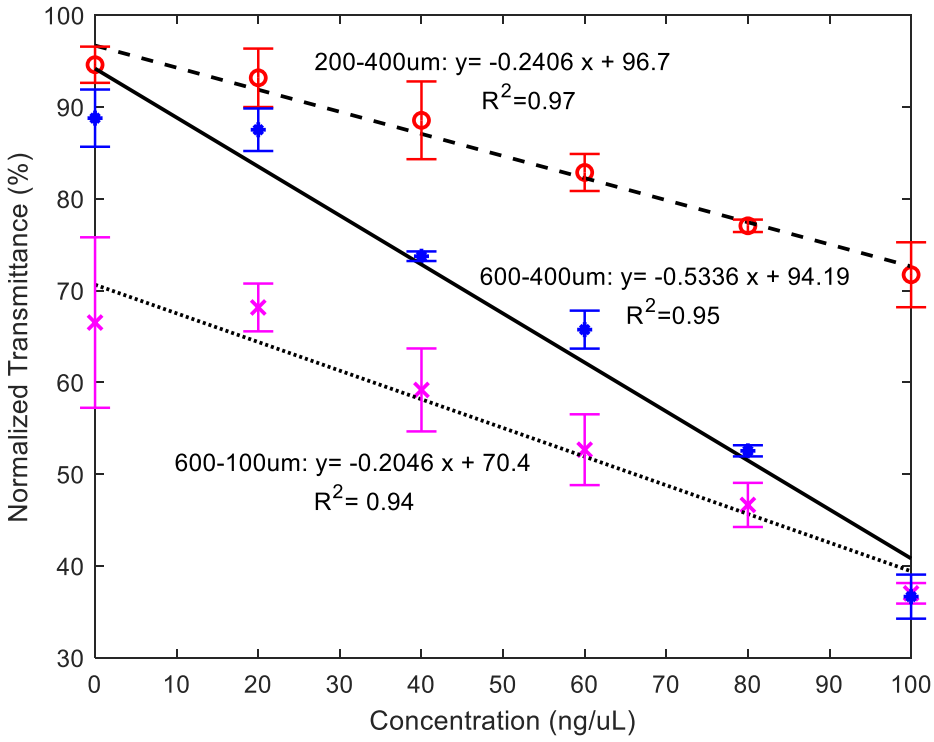

Fig. 2. *%T* against SARS-CoV-2 protein concentration at 275 nm for three combinations of *Tx-Rx* fiber diameter: 600-400 μm, 200–400 μm, and 600-100 μm.

modifications, such as tapered fibers or plasmonic surface enhancements (De Acha et al., 2021). Tapered fiber techniques, for instance, enhance light–sample interaction by reducing the core diameter to the micrometer scale, thereby increasing the penetration depth of the evanescent field (Borjikhani et al., 2025). In contrast, the present study employs standard multimode optical fibers without any tapering or plasmonic modifications. Nonetheless, similar studies using standard multimode fibers for glucose sensing and subcutaneous detection have reported results consistent with the findings of this work. In those studies, larger core diameters were found to improve detection performance for glucose concentrations and subcutaneous thicknesses within physiological ranges (Mustafa et al., 2016; Rodríguez-Rodríguez et al., 2025). This is likely due to the fact that larger fiber cores have a higher acceptance angle (θ_a), which allows a greater amount of light to enter and exit the fibers at both the transmitting and receiving ends (Willner, 2019), thereby mitigating attenuation effects such as absorption.

Further analysis on specificity using PCA score plots for all concentrations (0 ng/μL to 100 ng/μL in 20 ng/μL intervals), based on the full spectrum (200–1100 nm) and the single wavelength of 275 nm are illustrated in Fig. 3(a) and (b), respectively. Note that the optimized *Tx-Rx* (600–400 μm) was consistently employed in all subsequent measurements to ensure reliability and reproducibility across the PCA analyses. The PCA score plot for the full spectrum (Fig. 3(a)) shows that the first principal component accounts for 50 % of the variability in the *%T* spectra among SARS-CoV-2 protein, SARS-CoV protein, and rBmSXP protein. Redundancy between SARS-CoV-2 and SARS-CoV proteins is clearly observed, whereas the rBmSXP protein is successfully discriminated at all concentrations. When using the optimal single wavelength (275 nm), the PCA result (Fig. 3(b)) shows a marked improvement, with the explained variance increasing to 100 %. At this wavelength, all three proteins were completely differentiated across all concentrations. Notably, the SARS-CoV-2 protein data points are scattered according to concentration, indicating concentration-dependent variability. These findings not only enable discrimination between COVID-19 and other infectious diseases but also show potential for distinguishing between healthy individuals and patients with mild, moderate, or severe infections.

Specificity attribution becomes especially critical when using optical spectroscopy for pathogen detection. Unlike biosensor technologies where ligands selectively bind to the target analyte, the absence of such specific binding in optical spectroscopy method makes this approach heavily reliant on additional techniques such as statistical modelling and machine learning (Wu et al., 2022).The fundamental mechanism before applying these techniques involves several signal processing steps on the raw optical response that is captured by the detector. These pre-processing steps typically include interpolation, smoothing, baseline correction, and the calculation of first and second derivatives (Osco et al., 2022). The purposes of these techniques are to enhance spectral features, remove baseline noise, identify redundant peaks, and minimize baseline shifts. This approach is consistent with the work by B.F. Rumaling et al. on COVID-19 detection, in which signal smoothing using the Savitzky-Golay filter was performed prior to PCA analysis (Rumaling et al., 2023). In contrast, the present study demonstrates the stability of the optical system by applying the PCA directly to raw transmittance data without any prior pre-processing.

Principal component analysis (PCA) is classified as an unsupervised machine learning technique because it does not require class labels to analyze the data, unlike supervised learning algorithms (Younes et al., 2023). PCA is commonly used to reduce dimensionality, reveal hidden structures in the data, and visualize clusters based on variation. In this study, PCA is applied to differentiate between various protein types and concentrations. There was a previous study aimed to distinguish between infected and uninfected COVID-19 samples by combining PCA with a supervised method known as linear discriminant analysis (LDA), following signal pre-processing (Rumaling et al., 2023). Although the method achieved a specificity of 90 %, a notable limitation was identified. Since PCA does not incorporate class labels during dimensionality reduction, it may discard important features necessary for effective class separation using LDA. Therefore, selecting an appropriate number of principal components is crucial to preserve class-relevant information. A notable study applied supervised machine learning for COVID-19 detection using algorithms such as Support Vector Machine (SVM),

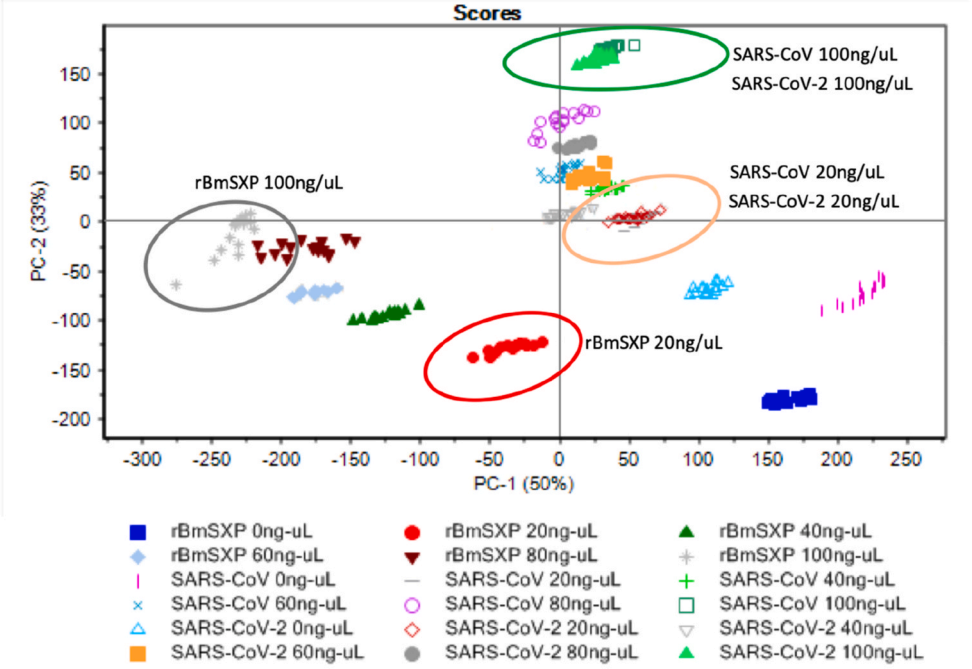

(a)

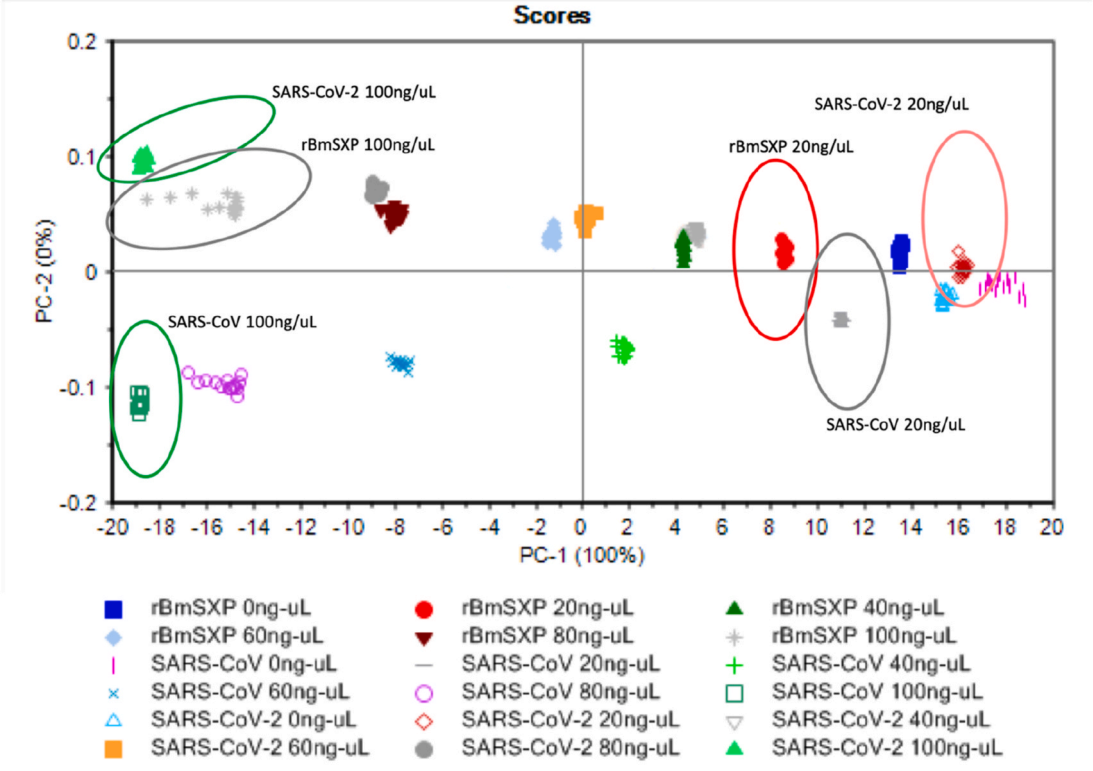

(b)

Fig. 3. PCA score plots of all concentrations for full spectrum (200 nm–1100 wavelength range), and (b) PCA score plots of all concentrations at the specific wavelength of 275 nm.

Random Forest, and Naive Bayes; however, it required spectral signal pre-processing prior to classification. In contrast, the present study demonstrates the ability to distinguish SARS-CoV-2 from SARS-CoV and rBmSXP proteins without any signal pre-processing (Coelho et al., 2024). In contrast, the present study demonstrates the ability to distinguish SARS-CoV-2 from SARS-CoV and rBmSXP proteins without any signal pre-processing. This highlights the potential of the optical spectroscopy approach, combined with unsupervised analysis, for rapid and reagent-free pathogen discrimination in clinical settings.

3.2. Measurement of clinical SARS-CoV-2 virus

The statistical data for 21 clinical COVID-19 samples based on the *Cq* values obtained from RT-qPCR measurements are summarized in Table 1. The *Cq* values range from 17 to 37, covering the spectrum from severe COVID-19 infection to the normal (non-infectious) category (van Rossum et al., 2023). In Table 1, the close proximity between the mean (27.49 ± 6.37) and the median (28) suggests that the dataset is relatively symmetrical or normally distributed. Fig. 4 illustrates the normalized transmittance (*%T*) spectra for samples with high, middle and low *Cq* values. A zoomed-in view in the inset reveals a spectral shift from 275 nm, where the peaks of the three *%T* curves do not align precisely at this wavelength. This shift may be attributed to the presence of various viral components beyond the S-protein, such as membrane proteins, RNA, and N-proteins. Notably, the sample with a lower *Cq* value, which indicates a higher viral load, demonstrates increased light absorption and consequently a lower *%T* reading. The lower transmittance observed in high viral load samples may also reflect increasing concentrations of viral RNA, nucleocapsid (N) proteins, or other virion components that absorb UV light. These findings align with the known absorption characteristics of nucleic acids and amino acids in viral proteins.

Additional absorption minima are also observed near 430 nm and 570 nm, consistent with a previous study that used UV–VIS–NIR spectroscopy on clinical SARS-CoV-2 virus samples obtained from swab tests (Rumaling et al., 2023). In contract, a study that measured SARS-CoV-2 virus in serum samples yielded different absorption features, with prominent peaks in the range from 780 nm to 1500 nm (Coelho et al., 2024). The variations in absorption spectra across sample types highlight the importance of selecting an appropriate detection wavelength. This emphasizes the relevance of the wavelength optimization process as described in Section 3.1, to ensure the most suitable wavelength is used in subsequent detection steps. While the sample size is modest ($n = 21$), it still captures a representative range of clinical severity, enabling a preliminary assessment of spectral trends across infection levels.

In the statistical analysis, the ratio of transmittance (%*T*) at 275 nm (associated with protein absorbance) to 970 nm (associated with water absorbance) was utilized for baseline normalization and offset correction (Mustafa et al., 2016b). A correlation analysis was performed to assess the relationship between the %*T* ratio (275 nm/970 nm) and the *Cq* values obtained from RT-qPCR as shown in Fig. 5. A positive correlation was obtained (Pearson's R = 0.6038, $p = 0.0037$), indicating a statistically significant linear association between the two measurements. The dispersion of data points around the regression line in Fig. 5 resulted in a root mean square error (RMSE) of 0.0775. Notably, the linear regression line does not intersect the origin, leading to an elevation of predicted transmittance values across the entire range. This offset contributes to the overestimation of optical signal intensity, particularly in samples with low *Cq* values.

Several factors may contribute to the limited predictive performance of the model. In particular, the optical signal may be affected by variables such as sample turbidity, background matrix effects, and variation in sample preparation - all of which are not accounted for in the present regression framework. Note that this study utilized native clinical SARS-CoV-2 samples, which were introduced directly into the optical detection system without any prior pre-processing steps. This approach was applied to maintain the samples' clinically relevant state and to assess the feasibility of the assay under conditions that closely resemble point-of-care settings. While this strategy enhances the real-world applicability of the method, it may also introduce matrix effects due to the presence of heterogeneous biological components, potentially affecting signal accuracy and reproducibility. Future optimization efforts should consider evaluating various sample pre-treatment strategies such as mild centrifugation, buffer exchange, or selective filtration to mitigate matrix-related interference while preserving clinical relevance. These improvements could further enhance the reliability and diagnostic performance of the optical assay in practical settings.

On the other hand, analytical performance may also be improved by integrating the optical spectroscopic platform with signal correction mechanisms or embedded modeling strategies for overestimation and measurement bias. Embedded correction mechanisms have proven effective in other spectroscopic platforms. For example, fNIRS systems have implemented auto-calibrated loops to continuously adjust offset currents caused by ambient light and tissue background, improving signal fidelity (Khan et al., 2025). Similarly, Gaussian Process models have been successfully employed to address correlated spectra in their transmission spectroscopy (Gibson et al., 2012). By integrating analogous embedded modeling or calibration modules in the optical platform such as baseline offset correction or systematic error modeling, it could substantially reduce overestimation bias and enhance performance in clinical samples. Additional improvements that could be achieved are by stratifying the dataset based on *Cq* thresholds (e.g., distinguishing between high and low viral load samples), where this may also help to reduce intra-group variability and improve interpretability. Furthermore, expanding the dataset beyond the current 21 samples is critical to increase statistical power and reinforce the robustness of the model.

Table 1
Statistical data of *Cq* value from RT-qPCR measurement ($n = 21$).

	Range	Mean ± SD	Median
Cq value from RT-qPCR measurements	17–37	27.49 ± 6.37	28

4. Conclusion

The proposed optical spectroscopy technique offers an advantage over conventional biosensors by being ligand-free and eliminating additional laboratory procedures, which are typically associated with ligand development, ligand immobilization, and surface functionalization. Furthermore, this study did not involve any pre-processing of raw optical transmittance signal, making it more robust than other studies utilizing similar optical spectroscopy approaches for COVID-19 detection. From the optimization study, the optimal detection wavelength for the SARS-CoV-2 protein was identified at 275 nm. A specificity of 100 % was achieved by comparing SARS-CoV-2 protein with other proteins, namely SARS-CoV and rBmSXP. The optimal *Tx–Rx* fiber size configuration was determined to be 600–400 μm. Clinical sample measurements of SARS-CoV-2 showed a correlation coefficient (R) of 0.6038 between the optical spectroscopy transmittance (*%T*) and the RT-qPCR *Cq* values, with statistically significant RMSE and *p*-values. These findings demonstrate that optical spectroscopy is a promising method for SARS-CoV-2 protein detection. However, this study can be further improved by placing greater emphasis on clinical measurement analysis, including background effect evaluation, performance metric assessment (e.g., sensitivity, limit of detection), and cross-reactivity testing with other respiratory diseases (e.g., influenza, respiratory syncytial virus), all supported by a larger clinical sample size (i.e., more than 21 samples). For future development toward a portable and compact free-space configuration, it is suggested to use light-emitting diodes (LED) at the optimal wavelength (e.g., 275 nm) along with a reference wavelength (e.g., 970 nm). On the receptor side, a photodiode that is optically coupled with a cosine corrector is recommended to enable light collection over a 180° field of view (as the cosine corrector has a θ_a of 180° or a numerical aperture of 1.0). In conclusion, the proposed optical spectroscopic method has strong potential for the detection of COVID-19 and other infectious diseases in future applications.

CRediT authorship contribution statement

Fatin Hamimi Mustafa: Writing – original draft, Visualization, Validation, Methodology, Investigation, Funding acquisition, Formal analysis, Data curation, Conceptualization. **Nik Yusnoraini Yusof:**

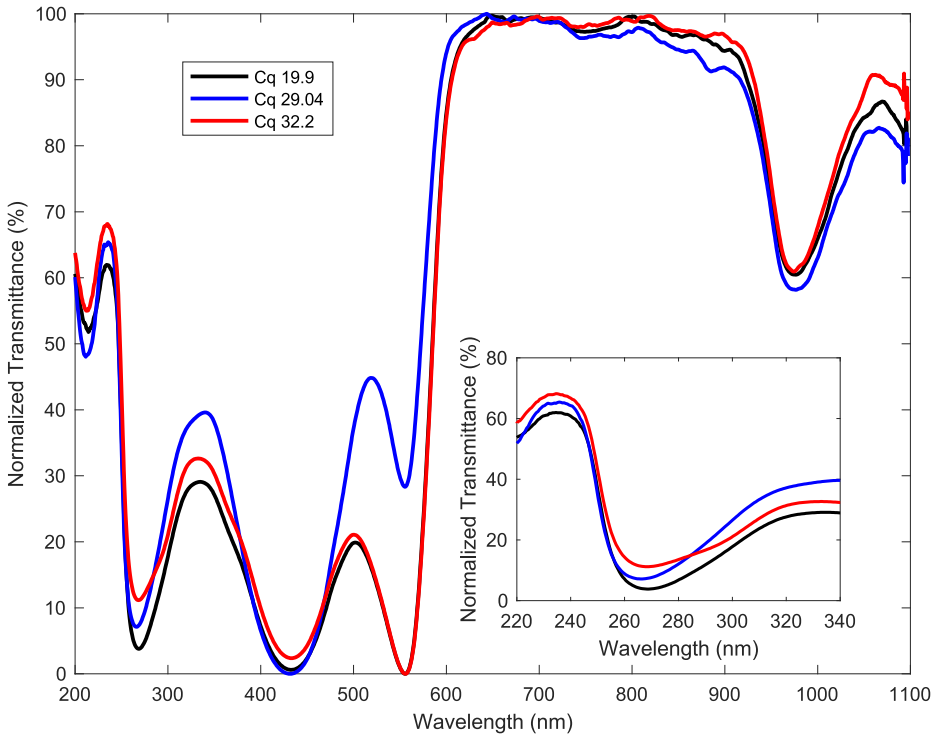

Fig. 4. Selected %*T* spectra of clinical SARS-CoV-2 samples based on *Cq* value.

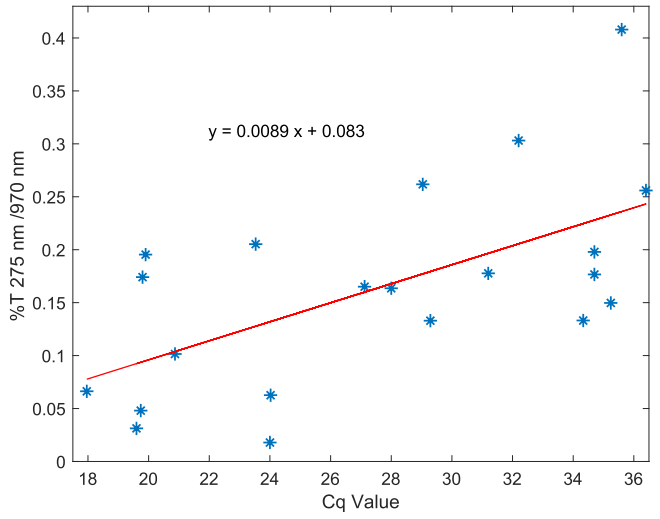

Fig. 5. Linear regression line of optical spectroscopy %*T* (ratio of 275 nm–970 nm) against RT-qPCR *Cq* value for SARS-CoV-2 virus measurements (total $n = 21$).

Resources, Methodology. **Mawaddah Mohd Azlan:** Methodology, Investigation. **Fariza Hanim Suhailin:** Visualization, Validation, Methodology. **Chan Yean Yean:** Supervision, Resources. **Nik Mohd Noor Nik Zuraina:** Methodology, Investigation. **Mohd Zulkifli Salleh:** Resources, Methodology, Investigation. **Hironaga Uchida:** Writing – review & editing, Resources, Funding acquisition. **Irneza Ismail:** Writing – review & editing, Funding acquisition. **Rosline Hassan:** Software, Resources. **Raja Kamarulzaman Raja Ibrahim:** Writing – review & editing, Supervision, Software, Formal analysis. **Mohd Adzir Mahdi:** Validation, Supervision.

Informed consent statement

The patients of COVID-19 provided the consent to use the data for research. The clinical sample collection procedure and research were approved by the Human Research Ethics Committee (JEPeM) of Hospital Universiti Sains Malaysia (Protocol No.: USM/JEPeM/COVID19-44).

Declaration of competing interest

The authors declare that they have no known competing financial interests or personal relationships that could have appeared to influence the work reported in this paper.

Acknowledgement

The authors would like to thank to the funder, the ASEAN University Network/Southeast Asia Engineering Education Development Network (JICA Project for AUN/SEED-Net), Special Program for Research against COVID-19 (304/CIPPM/6150185/A119). The authors are grateful to the funder. We would like to thank Dr. Syaida Hanasil for PCA contribution. Thank you also goes to Amy Amilda Anthony and Basyirah Ghazali for their contribution throughout this project.

Data availability

The authors do not have permission to share data.

References

Al Ahmad, M., Olule, L.J., Meetani, M., Sheikh, F.A., Al Blooshi, R., Panicker, N.G., Mustafa, F., Rizvi, T.A., 2021. Detection of SARS-CoV-2 in COVID-19 patient nasal swab samples using signal processing. IEEE Journal of Selected Topics in Signal Processing 16 (2), 164–174. https://doi.org/10.1109/JSTSP.2021.3130324.

Antosiewicz, J.M., Shugar, D., 2016. UV-Vis spectroscopy of tyrosine side-groups in studies of protein structure. Part 2: selected applications. Biophys. rev. 8 (2), 163–177. https://doi.org/10.1007/s12551-016-0201-5.

Borjikhani, P., Granpayeh, N., Zibaii, M.I., 2025. High sensitivity tapered fiber refractive index biosensor using hollow gold nanoparticles. Sci. Rep. 15 (1), 1458. https://doi.org/10.1038/s41598-025-85739-z.

Coelho, B.F.O., Nunes, S.L.P., de França, C.A., dos Santos Costa, D., do Carmo, R.F., Prates, R.M., Simas Filho, E.F., Ramos, R.P., 2024. On the feasibility of Vis–NIR spectroscopy and machine learning for real time SARS-CoV-2 detection. Spectrochim. Acta Mol. Biomol. Spectrosc. 308, 123735. https://doi.org/10.1016/j.saa.2024.123735.

Cucinotta, D., Vanelli, M., 2020. WHO declares COVID-19 a pandemic. Acta Biomed.: Atenei Parmensis 91 (1), 157. https://doi.org/10.23750/abm.v91i1.9397.

De Acha, N., Socorro-Leránoz, A.B., Elosúa, C., Matías, I.R., 2021. Trends in the design of intensity-based optical fiber biosensors (2010–2020). Biosensors 11 (6), 197. https://doi.org/10.3390/bios11060197.

Desjardins, P., Conklin, D., 2010. NanoDrop microvolume quantitation of nucleic acids. J. Vis. Exp. 45, 2565. https://doi.org/10.3791/2565.

Di Domenico, M., De Rosa, A., Boccellino, M., 2021. Detection of SARS-COV-2 proteins using an ELISA test. Diagnostics 11 (4), 698. https://doi.org/10.3390/diagnostics11040698.

Edelhoch, H., 1967. Spectroscopic determination of tryptophan and tyrosine in proteins. Biochemistry 6 (7), 1948–1954. https://doi.org/10.1021/bi00859a010.

Garcia, G.A., Lord, A.R., Santos, L.M., Kariyawasam, T.N., David, M.R., Couto-Lima, D., Tátila-Ferreira, A., Pavan, M.G., Sikulu-Lord, M.T., Maciel-de-Freitas, R., 2022. Rapid and non-Invasive detection of Aedes aegypti Co-infected with Zika and Dengue viruses using near infrared spectroscopy. Viruses 15 (1), 11. https://doi.org/10.3390/v15010011.

Gibson, N., Aigrain, S., Roberts, S., Evans, T., Osborne, M., Pont, F., 2012. A Gaussian process framework for modelling instrumental systematics: application to transmission spectroscopy. Mon. Not. Roy. Astron. Soc. 419 (3), 2683–2694. https://doi.org/10.1111/j.1365-2966.2011.19915.x.

Gössling, S., Scott, D., Hall, C.M., 2020. Pandemics, tourism and global change: a rapid assessment of COVID-19. J. Sustain. Tourism 29 (1), 1–20. https://doi.org/10.1080/09669582.2020.1758708.

Hardenbrook, N.J., Zhang, P., 2022. A structural view of the SARS-CoV-2 virus and its assembly. Curr Opin Virol. 52, 123–134. https://doi.org/10.1016/j.coviro.2021.11.011.

Howard, M.W., Travanty, E.A., Jeffers, S.A., Smith, M., Wennier, S.T., Thackray, L.B., Holmes, K.V., 2008. Aromatic amino acids in the juxtamembrane domain of severe acute respiratory syndrome coronavirus spike glycoprotein are important for receptor-dependent virus entry and cell-cell fusion. J. Virol. 82 (6), 2883–2894. https://doi.org/10.1128/JVI.01805-07.

Jacques, S.L., 2013. Optical properties of biological tissues: a review. Phys. Med. Biol. 58 (11), R37. https://doi.org/10.1088/0031-9155/58/11/R37.

Khan, I., Haleem, A., Javaid, M., 2020. Analysing COVID-19 pandemic through cases, deaths, and recoveries. J. Oral Biol. Craniofac. Res. 10 (4), 450–469. https://doi.org/10.1016/j.jobcr.2020.08.003.

Khan, S.S., Padhi, P.K., Wani, S.A., Ahmad, M., Somappa, L., Malik, S., 2025. An embedded auto-calibrated offset current compensation technique for PPG/fNIRS system. IEEE Embedded Systems Letters. https://doi.org/10.1109/LES.2025.3550393.

Kitane, D.L., Loukman, S., Marchoudi, N., Fernandez-Galiana, A., El Ansari, F.Z., Jouali, F., Badir, J., Gala, J.-L., Bertsimas, D., Azami, N., 2021. A simple and fast spectroscopy-based technique for Covid-19 diagnosis. Sci. Rep. 11 (1), 16740. https://doi.org/10.1038/s41598-021-95568-5.

Lee, S., Bi, L., Chen, H., Lin, D., Mei, R., Wu, Y., Chen, L., Joo, S.-W., Choo, J., 2023. Recent advances in point-of-care testing of COVID-19. Chem. Soc. Rev. 52 (24), 8500–8530. https://doi.org/10.1039/D3CS00709J.

Lino, C., Barrias, S., Chaves, R., Adega, F., Martins-Lopes, P., Fernandes, J., 2022. Biosensors as diagnostic tools in clinical applications. Biochim. Biophys. Acta Rev. Canc 1877 (3), 188726. https://doi.org/10.1016/j.bbcan.2022.188726.

Liu, M., Li, Q., Zhou, J., Ai, W., Zheng, X., Zeng, J., Liu, Y., Xiang, X., Guo, R., Li, X., 2020. Value of swab types and collection time on SARS-COV-2 detection using RT-PCR assay. J. Virol. Methods 286, 113974. https://doi.org/10.1016/j.jviromet.2020.113974.

Luporini, R.L., Pott-Junior, H., Leal, M.C.B.D.M., Castro, A., Ferreira, A.G., Cominetti, M. R., de Freitas Anibal, F., 2021. Phenylalanine and COVID-19: Tracking disease severity markers. Int. Immunopharmacol. 101, 108313. https://doi.org/10.1016/j.intimp.2021.108313.

Mahmoudinobar, F., Britton, D., Montclare, J.K., 2021. Protein-based lateral flow assays for COVID-19 detection. Protein Eng. Des. Sel. 34, gzab010. https://doi.org/10.1093/protein/gzab010.

Minamikawa, T., Koma, T., Suzuki, A., Mizuno, T., Nagamatsu, K., Arimochi, H., Tsuchiya, K., Matsuoka, K., Yasui, T., Yasutomo, K., 2021. Quantitative evaluation of SARS-CoV-2 inactivation using a deep ultraviolet light-emitting diode. Sci. Rep. 11 (1), 5070. https://doi.org/10.1038/s41598-021-84592-0.

Mojsoska, B., Larsen, S., Olsen, D.A., Madsen, J.S., Brandslund, I., Alatraktchi, F.A.a., 2021. Rapid SARS-CoV-2 detection using electrochemical immunosensor. Sensors 21 (2), 390. https://doi.org/10.3390/s21020390.

Mustafa, F.H., Bek, E.J., Huvanandana, J., Jones, P.W., Carberry, A.E., Jeffery, H.E., Jin, C.T., McEwan, A.L., 2016. Length-free near infrared measurement of newborn malnutrition. Sci. Rep. 6 (1), 36052. https://doi.org/10.1038/srep36052.

Mustafa, F.H., Ismail, I., Munawar, A.A.Z.A., Basir, B.A., Shueb, R.H., Irekeola, A.A., Ismail, W.Z.W., Jamaludin, J., Balakrishnan, S.R., Sahrim, M.a., 2023. A review on current diagnostic tools and potential optical absorption spectroscopy for HFMD detection. Anal. Biochem. 683, 115368. https://doi.org/10.1016/j.ab.2023.115368.

Osco, L.P., Furuya, D.E.G., Furuya, M.T.G., Correa, D.V., Goncalvez, W.N., Junior, J.M., Borges, M., Blassioli-Moraes, M.C., Michereff, M.F.F., Aquino, M.F.S., 2022. An impact analysis of pre-processing techniques in spectroscopy data to classify insect-damaged in soybean plants with machine and deep learning methods. Infrared Phys. Technol. 123, 104203. https://doi.org/10.1016/j.infrared.2022.104203.

Rodríguez-Rodríguez, W.E., Rodríguez-Rodríguez, A.J., Juárez-Saldivar, A., Zamarreño, C., Matias, I., 2025. Low-cost optical fiber multimode interference biosensor based on a glucose sensitive Glucose-Oxidase enzyme thin-film. Sens. Acutators Rep. 9, 100267. https://doi.org/10.1016/j.snr.2024.100267.

Rumaling, M.I., Chee, F.P., Bade, A., Chang, J.H.W., Goh, L.P.W., Juhim, F., 2023. Detection of coronavirus in viral transport media using ultraviolet and near-infrared absorbance spectra and Pattern recognition model. https://doi.org/10.21203/rs.3.rs-3684212/v1.

Sakudo, A., Baba, K., Ikuta, K., 2012. Discrimination of influenza virus-infected nasal fluids by Vis-NIR spectroscopy. Clin. Chim. Acta 414, 130–134. https://doi.org/10.1016/j.cca.2012.08.022.

Sakudo, A., Tsenkova, R., Onozuka, T., Morita, K., Li, S., Warachit, J., Iwabu, Y., Li, G., Onodera, T., Ikuta, K., 2005. A novel diagnostic method for human immunodeficiency virus type-1 in plasma by near-infrared spectroscopy. Microbiol. Immunol. 49 (7), 695–701. https://doi.org/10.1111/j.1348-0421.2005.tb03648.x.

Sapuan, S., Ilyas, R., Harussani, M., 2025. Recent global scenarios during COVID-19 pandemic outbreak. Advanced Composites. Springer, pp. 1–17. https://doi.org/10.1007/978-3-031-71448-1.

Selinger, K., Fung, E.N., Bryan, P., 2014. Bioanalytical Method Validation and Bioanalysis in Regulated Settings, Specification of Drug Substances and Products. Elsevier, pp. 325–363. https://doi.org/10.1016/B978-0-08-098350-9.00016-3.

Shim, J.-E., Kim, Y.J., Choe, J.-H., Lee, T.G., You, E.-A., 2022. Single-Nanoparticle-based digital SERS sensing platform for the accurate quantitative detection of SARS-CoV-2. ACS Appl. Mater. Interfaces 14 (34), 38459–38470. https://doi.org/10.1021/acsami.2c07497.

Siu, R.H., Jesky, R.G., Fan, Y.-J., Au-Yeung, C.C., Kinghorn, A.B., Chan, K.-H., Hung, I.F.-N., Tanner, J.A., 2024. Aptamer-mediated electrochemical detection of SARS-CoV-2 nucleocapsid protein in saliva. Biosensors 14 (10), 471. https://doi.org/10.3390/bios14100471.

Spinelli, A., Pellino, G., 2020. COVID-19 pandemic: perspectives on an unfolding crisis. Journal of British Surgery 107 (7), 785–787. https://doi.org/10.1002/bjs.11627.

Tkachenko, N.V., 2006. Optical Spectroscopy: Methods and Instrumentations. Elsevier.

van Rossum, C., Meijer, C., van Weerdenburg, I.J., Bowles, E.C., Rovers, C.P., Ten Oever, J., Stol, K., van der Geest, N.D., McCall, M.B., Tostmann, A., 2023. Low SARS-CoV-2 Cq values in healthcare workers with symptomatic COVID-19 infections, regardless of symptom severity, The Netherlands, January to August 2022. Euro Surveill. 28 (4), 2300007. https://doi.org/10.2807/1560-7917.ES.2023.28.4.2300007.

Willner, A., 2019. Optical Fiber Telecommunications. Academic Press.

Wu, W., Wang, L., Yang, Y., Du, W., Ji, W., Fang, Z., Hou, X., Wu, Q., Zhang, C., Li, L., 2022. Optical flexible biosensors: from detection principles to biomedical applications. Biosens. Bioelectron. 210, 114328. https://doi.org/10.1016/j.bios.2022.114328.

Wu, Y., Yu, Q., Joung, Y., Jeon, C.S., Lee, S., Pyun, S.H., Joo, S.-W., Chen, L., Choo, J., 2023. Highly uniform self-assembly of gold nanoparticles by butanol-induced dehydration and its sers applications in SARS-CoV-2 detection. Anal. Chem. 95 (34), 12710–12718. https://doi.org/10.1021/acs.analchem.3c01348.

Yang, Y., Peng, Y., Lin, C., Long, L., Hu, J., He, J., Zeng, H., Huang, Z., Li, Z.-Y., Tanemura, M., 2021. Human ACE2-functionalized gold "virus-trap" nanostructures for accurate capture of SARS-CoV-2 and single-virus SERS detection. Nano-Micro Lett. 13, 1–13. https://doi.org/10.1007/s40820-021-00620-8.

Yano, T.-a., Kajisa, T., Ono, M., Miyasaka, Y., Hasegawa, Y., Saito, A., Otsuka, K., Sakane, A., Sasaki, T., Yasutomo, K., 2022. Ultrasensitive detection of SARS-CoV-2 nucleocapsid protein using large gold nanoparticle-enhanced surface plasmon resonance. Sci. Rep. 12 (1), 1060. https://doi.org/10.1038/s41598-022-05036-x.

Yesudhas, D., Srivastava, A., Gromiha, M.M., 2021. COVID-19 outbreak: history, mechanism, transmission, structural studies and therapeutics. Infection 49 (2), 199–213. https://doi.org/10.1007/s15010-020-01516-2.

Younes, K., Kharboutly, Y., Antar, M., Chaouk, H., Obeid, E., Mouhtady, O., Abu-Samha, M., Halwani, J., Murshid, N., 2023. Application of unsupervised machine learning for the evaluation of aerogels' efficiency towards ion removal—a principal component analysis (PCA) approach. Gels 9 (4), 304. https://doi.org/10.3390/gels9040304.

Zhao, X., Chen, H., Wang, H., 2021. Glycans of SARS-CoV-2 spike protein in virus infection and antibody production. Front. Mol. Biosci. 8, 629873. https://doi.org/10.3389/fmolb.2021.629873.

Zhou, H., Yang, J., Zhou, C., Chen, B., Fang, H., Chen, S., Zhang, X., Wang, L., Zhang, L., 2021. A review of SARS-CoV2: compared with SARS-CoV and MERS-CoV. Front. Med. 8. https://doi.org/10.3389/fmed.2021.628370.